THE JOURNAL OF PHYSICAL CHEMISTRY B

B: Liquids; Chemical and Dynamical Processes in Solution

Improvement of the ReaxFF Description for Functionalized Hydrocarbon/Water Weak Interactions in the Condensed Phase

Weiwei Zhang, and Adri C.T. van Duin

J. Phys. Chem. B, **Just Accepted Manuscript** • DOI: 10.1021/acs.jpcb.8b01127 • Publication Date (Web): 08 Mar 2018

ACS Publications

is published by the American Chemical Society. 1155 Sixteenth Street N.W., Washington, DC 20036

Improvement of the ReaxFF Description for Functionalized Hydrocarbon/Water Weak Interactions in the Condensed Phase

Weiwei Zhang, Adri C. T. van Duin*

Department of Mechanical and Nuclear Engineering, Pennsylvania State University, University Park, Pennsylvania 16802, United States

Abstract

The ReaxFF protein reactive force field (protein-2013) has been successfully employed to simulate the biomolecules and membrane fuel cells, but it inaccurately describes the weak interaction of functionalized hydrocarbon/water molecules in condensed phase, especially for the density. In this article, the development of a ReaxFF force field (CHON-2017_weak) on the basis of protein-2013 is presented that improves the weak interaction description between carbon, hydrogen, oxygen and nitrogen. To examine the quality of the force field, we performed a series of molecular dynamics simulations with model systems. These simulations, describing density trends for pure and mixture compound systems, demonstrate that CHON-2017_weak force field predictions are in good agreement with experimental data. Furthermore, ReaxFF can also describe the phase separation in hexane-water mixture and dissolution of ethanol or tetramethylammonium (TMA) in liquid water. To validate it in the application of membrane fuel cells, we studied structural property and degradation mechanism of TMA

in alkaline aqueous solution, as well as some typical chemical reactions for small compounds. On the basis of our results, an additional reaction pathway is proposed for the degradation of TMA, which seems to be more energetically favorable compared to the main mechanism predicted from quantum mechanics calculations.

1 Introduction

Computer simulations provide a powerful tool for exploring the properties of molecules and materials.[1-3] Currently, there are two main strategies for the simulations at the atomistic level, one is the method based on quantum mechanics (QM) referring to complex Schrodinger equation and the other is classical mechanics method, namely solving Newton's equation. In principle, the QM methods can accurately obtain the detailed information of the system, such as configurations, electronic structures, energies and vibrations. Unfortunately, those methods, such as *ab initio* molecular dynamics (AIMD) simulations and density functional theory (DFT), only allow one to treat the systems less than several hundreds of atoms due to the extremely high computational cost. Such limitation often excludes the QM methods from simulating the structural and dynamics properties of the larger systems at nanoscale. However, the empirical force field (FF) based strategies make it possible to investigate the system at such large size and/or time scales.[1] For example, they are able to simulate the system much larger than 10^6 atoms at nanosecond time scale.

During the past decades, numerous empirical FF methods have been developed to treat different type systems.[3-4] For instance, the popular general FF is so-called MM potentials developed by Allinger's group (i.e. MM2 and MM3 etc.)[5-6], which is widely used to study the small hydrocarbons and functionalized organic molecules due to the good

predictions of geometries, as well as conformational energy differences. UFF[7] and Dreiding[8] are also good examples of generic FFs. They contain parameters of most elements in the periodic table and thus have a broad applicability. Other popular FFs such as GROMOS[9], AMBER[10] and CHARMM[11] are usually employed to simulate the biomolecules while OPLS[12] and COMPASS[13] were developed to study the condensed matter like polymer, metal and metal oxides. Moreover, many specific potentials have been developed to describe a particular target system. For instance, the most popular water models are TIP3P, SPC/E, TIP4P/2005 etc.[14-16]

All the above traditional FF methods have been developed on the basis of rigid connectivity of the atoms and they thus fail to describe the chemical reactions, such as bond breaking and bond formation during the MD simulations. To incorporate the chemical reactions, various reactive potentials were developed based on the bond order concepts,[17] such as reactive empirical bond order (REBO) potential,[18] charged-optimized many-body (COMB) potential[19] and the ReaxFF reactive force field.[1, 20] In particular, the ReaxFF has demonstrated its ability to transfer to a wide variety of elements and has been applied to simulate the complicated chemical reactions in different phases, such as gas and condensed phases, as well as at the interface between the phases.[21-23]

There are currently two major development branches of parameter sets in the ReaxFF development tree,[1] namely the combustion and the aqueous branches. ReaxFF has high intra-transferability within one branch - they share the same general and first-row element parameters. Regarding the aqueous branch, it contains amongst others, the interaction between water molecules and a series of metal oxides (SiO_2,[24] CuO,[25] ZnO,[26] Clay,[27] etc.), as well as protein/DNA.[28] For the protein force field (protein-2013) in the water branch,

the first-row element parameters of carbon were initially developed on the basis of C/H/O-2008 combustion force field[29] while all of the parameters of oxygen and hydrogen came from the first generation water force field.[30] The first-row element parameters of nitrogen were transferred from the force field developed to simulate glycine in aqueous solution.[31] Based on this, the protein force field was extended to explore more complex biomolecules.[28] Recently, it was also successfully used to investigate the anion exchange membrane containing quaternary ammonium.[32] From the studies of three functionalized poly(phenylene oxide) anion exchange membranes (AEMs), we demonstrated the diffusion constants of both hydroxide ion and water can be successfully predicted with ReaxFF simulations. Furthermore, the degradation study of membrane showed the large-scale substituent group on hydrophilic cation has good chemical stability. However, we also note some issues for the protein-2013 force field. For example, the density of liquid water is underestimated while the densities of hydrocarbon systems are overestimated in the comparison of experimental data. In this paper, we re-optimized the force field parameters regarding carbon (C), hydrogen (H), oxygen (O) and nitrogen (N) to address the issues in the description of functionalized hydrocarbon/water weak interaction in the condensed phase, and the new developed force field is called CHON-2017_weak. At the same time, all the good features of protein-2013 force field should also be retained such as the dynamical and structural properties of water, and reactions as described in previous works.[30, 32] To validate the quality of CHON-2017_weak force field in the application of membrane fuel cell systems, we took tetramethylammonium (TMA), which is a common side chain cation group in the design of anion exchange membrane fuel cells, for an example system to study its structural

property and degradation in aqueous solution.

This paper is organized as follows: In Section 2, we will describe the force field development briefly and MD simulation details. The validation and discussion are given in Section 3, while the conclusions are summarized in Section 4.

2 Computational methods

2.1 ReaxFF force field development

The ReaxFF energy can be generally expressed as[29]

$$E_{system} = E_{bond} + E_{val} + E_{tor} + E_{over} + E_{under} + E_{lp} + E_{vdw} + E_{coul} + E_{HB} . \quad (1)$$

Here the total energy of the system consists of bond, three-body angle and four-body torsional angle energies, over-coordination, under-coordination and lone pair energies, and non-bonded energies such as the contribution of van der Waals and Coulomb interactions, as well as the hydrogen bond contribution. For more details of the ReaxFF potential forms we refer to van Duin and Chenoweth publications.[20, 29] Generally, the ReaxFF force field parameters are trained against QM data using a successive one-parameter search method.[33] As mentioned above, the protein-2013 force field has been successful in the study of reactions evolving the biomolecule and membrane fuel cell systems, but it does not properly describe the weak interactions in functionalized hydrocarbon/water system. For this reason, we mainly focus on retraining the parameters related to such weak interactions to improve the description of the binding energy of molecule pairs. In detail, we re-optimized the element parameters regarding the van der Waals (VDW) force and electron equilibration method (EEM) Coulomb terms, as well as the hydrogen bonding terms. All the parameters describe the weak interaction of the carbon/hydrogen/oxygen (C/H/O) atom pairs. For example, we added the equation of

state of cyclohexane in our previous train set to improve the density description of the hydrocarbon system, and the binding energies of water clusters were retrained to reproduce the density of liquid water. Meanwhile, the chemical reactions regarding the systems containing nitrogen (N) were also included in the re-parameterization procedure. Given the significant parameter correlation in ReaxFF, the changes of these parameters also affect the bond order of the atom pairs, making it also necessary to retrain the bond and angle parameters. The new parameters of CHON-2017_weak force field are included in the Supporting Information in the standard ReaxFF force field format and can be used with ADF,[34] LAMMPS[35] and the standalone ReaxFF code. In this work, we employed standalone ReaxFF code to optimize the force field parameters and validate the quality of the CHON-2017_weak force field for the small molecules, while the long term MD simulations for various large modeling systems were performed with the parallel ADF-2016 package mentioned above.

2.2 Molecular Dynamics Simulations

Using the CHON-2017_weak force field parameters, a series of MD simulations were carried out to validate its performance. To evaluate the densities of the liquid systems, we firstly placed the molecules randomly in a big simulation box at a low density (i.e. 0.1g/cm^3) followed by equilibration with a fixed cell. After that, we compressed the box during the simulation to get a density close to the experiment result. In the end, a 500 ps NPT/MD simulation at room temperature was performed to equilibrate the system and the density of the system was obtained by averaging the last 400 ps data. For the amino acid crystals the initial configurations were from experimental crystal structures[36] and the

temperature was controlled at 100K to minimize the thermal fluctuation effect during the NPT/MD simulations. Besides, in order to get the structural and dynamic properties of liquid water (i.e. the radial distribution function (RDF) and self-diffusion constant), as well as the structural property and chemical reactions of TMA/OH/water mixture, we performed a 500 ps NVT/MD simulation for the system. For all current ReaxFF MD simulations, the time step is 0.25 fs and the Berendsen thermostat was used with a pressure and temperature damping constant of 2500 and 100 fs for the NPT and NVT MD simulations, respectively. In the reaction mechanism study, the temperature was set to 0.1K in the ReaxFF calculations in order to directly compare with the QM results, which were calculated at 0 K generally.

3 Results and Discussion

3.1 Validation for water

We have known that the density of bulk water predicted with the first generation ReaxFF water force field is around 0.90 g/cm^3, which is significantly underestimated compared to the experimental result.[37] Therefore, the oxygen and hydrogen element, bond, angle and hydrogen bonding parameters were re-parameterized to improve the description of the binding energies of water clusters. As discussed in the following section, the CHON-2017_weak force field reproduces the experimental density well.

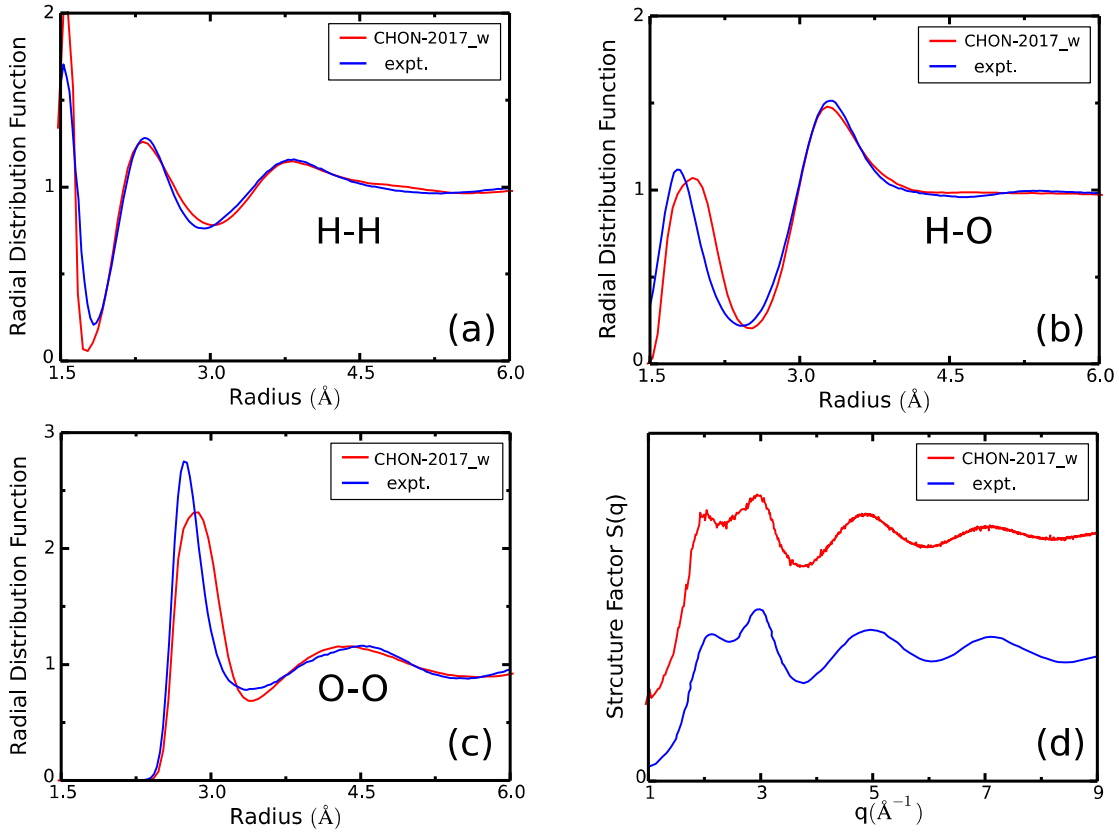

Figure 1: The predicted (CHON-2017_weak force field) and experimental radial distribution functions for (a) H-H, (b) H-O and (c) O-O of liquid water, respectively. (d) The predicted and experimental structure factors (arb. unit) of liquid water, the results have been shifted vertically for clarity.

In order to validate the quality of CHON-2017_weak force field in the description of structural property of liquid water, we firstly calculated the radial distribution functions (RDFs) of water for the system with 500 water molecules and showed them in Figure 1 (The H-H, H-O and O-O RDFs were plotted in Figure 1a, Figure 1b and Figure 1c, respectively). From the comparisons, it is found the CHON-2017_weak force field generally reproduces the experimental RDFs for liquid water.[38] We should mention that although the first peak of predicted O-O RDF shows a right shift with slightly smaller

intensity, indicating the liquid water in ReaxFF is slightly less structured than the experimental observation, However, all the ReaxFF peaks of structure factor are in good agreement with the experimental value[39] as shown in Figure 1d. Here, the Sayre-Ten Eyck approach was employed to calculate the structure factor, which can be obtained numerically on the basis of discrete Fourier transform:[40]

$$F(q) = \frac{V}{N_X N_Y N_Z} \sum_{j_X=0}^{N_X-1} \sum_{j_Y=0}^{N_Y-1} \sum_{j_Z=0}^{N_Z-1} \rho(j_X, j_Y, j_Z) \times \exp[2i\pi(hj_X + kj_Y + lj_Z)], \qquad (2)$$

where $q=ha^*+kb^*+lc^*$, hkl and $a^*b^*c^*$ are Miller indices and reciprocal lattice vectors, respectively. V stands for the volume of the simulation box and N_X, N_Y, N_Z are the numbers of grid points along each of the axes. $\rho(j_X, j_Y, j_Z)$ represents the density distribution at the grid of (j_X, j_Y, j_Z), which equals to 1 or 0 depending on whether an oxygen is found or not at the grid.

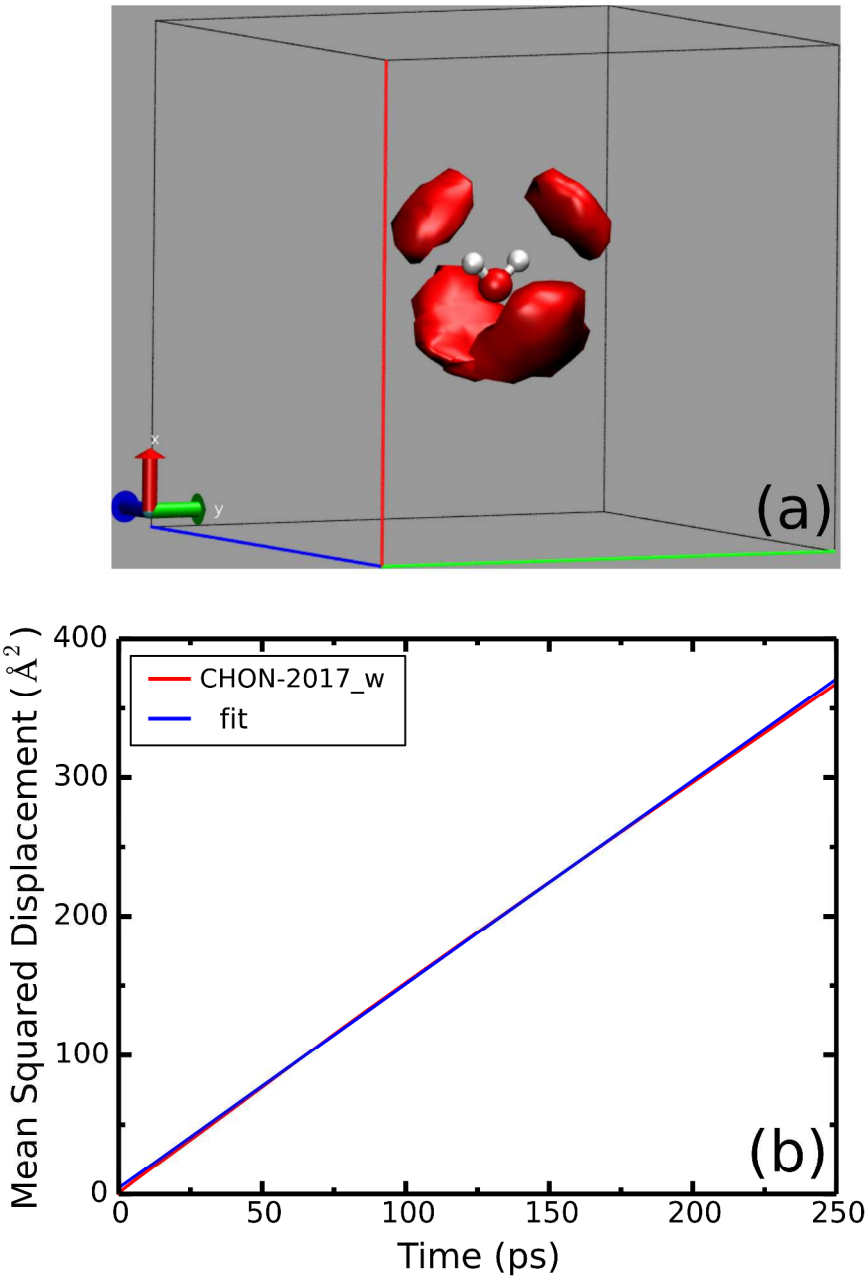

Figure 2: (a) The predicted spatial density function with CHON-2017_weak force field for the first solvation shell water molecules around a center water. The shaded red regions represent the probability of finding the oxygen atom of solvating water molecule. Oxygen is shown in red, and hydrogen in white. (b) The predicted and fitted mean square displacements as a function of simulation time.

To elucidate the solvation structure of water molecule further, we calculated the spatial distribution function (SDF), this is visualized in Figure 2a. We found the SDF of the oxygen atom in the solvating water molecule, which are around a center water molecule within 3.3 Å, is in good agreement with the experimental observation.[41] Moreover, another very important property of liquid water is the self-diffusion constant of water, which can be estimated from the mean square displacement (MSD) and Einstein relation.[37] The time dependence of MSD is displayed in Figure 2b, and the slope is related to the diffusion constant directly. The fitted self-diffusion constant is 0.25 $Å^2$/ps, which is also in good agreement with the experimental data of 0.24 $Å^2$/ps. On the basis of the results of liquid water density, structural and dynamic properties, as shown in Figure 1 and Figure 2, the CHON-2017_weak force field is indeed able to give good description of liquid water.

3.2 Density of pure compound model

n-alkane As mentioned above, the protein-2013 force field overestimates the densities of hydrocarbon systems caused by the inaccurate description of the intermolecular weak interactions, we therefore re-parameterized the carbon-carbon and carbon-hydrogen interactions, especially the VDW parameters for the weak interactions. For the purpose of comparison, we list the simulated densities of a series of liquid saturated hydrocarbon compounds predicted by protein-2013 and CHON-2017_weak force fields in Table 1, as well as the experimental data. All these simulations were performed on periodic boxes containing 200 copies of the n-alkane molecule. It is found that the densities increase with the elongated length of carbon chain for both protein-2013 and CHON-2017_weak predictions. This trend is consistent with the experimental observation. However, the

comparison of the protein-2013 and CHON-2017_weak force field results with the experimental data clearly shows that the CHON-2017_weak force field significantly improves the density description. Overall, the predicted densities with CHON-2017_weak force field are in good agreement with the experiment results. However, the protein-2013 force field overestimates all the densities of saturated hydrocarbons with up to ~ 40%.

Table 1. Densities of the n-alkane Compounds at 298.15K.

System	Chemical formula	protein-2013	CHON-2017_weak	expt.
pentane	C_5H_{12}	0.99	0.63	0.62[42]
hexane	C_6H_{14}	1.02	0.67	0.66[43]
heptane	C_7H_{16}	1.04	0.69	0.68[43]
octane	C_8H_{18}	1.05	0.71	0.70[43]
decane	$C_{10}H_{22}$	1.08	0.74	0.73[43]

Aromatic hydrocarbons Besides saturated hydrocarbon compounds in which all the carbon-carbon bonds are sigma bonds, aromatic hydrocarbons are also the common organic compounds in nature. This type of compounds with a ring of resonance bonds exhibits more chemical stability than other geometric or connective arrangements with the same carbon atom. Since the bond order between a pair of atoms can be obtained from the interatomic distance directly, the ReaxFF can also describe the atom in different chemical environment with the same element parameters. For example, it can capture the transitions between sigma, pi and triple bond character for carbon during the MD simulation. Table 2 summarizes some typical aromatic hydrocarbon compounds, in which

carbon atoms are saturated or unsaturated. Similar to the alkanes discussed in the previous section, these simulations were performed on periodic boxes containing 200 copies of the aromatic compound. Compared to the simulated results with protein-2013 force field, it indicates the CHON-2017_weak force field significantly improves in the density description, which agrees with the experiment.

Table 2. Densities of the Aromatic Hydrocarbons at 298.15K.

System	Chemical formula	protein-2013	CHON-2017_weak	expt.
toluene	C_7H_8	1.25	0.89	0.86[44]
naphthalene	$C_{10}H_8$	1.38	1.09	1.14[45]
styrene	C_8H_8	1.29	0.96	0.91[46]
ethylbenzene	C_8H_{10}	1.24	0.90	0.86[47]

Hydrocarbon oxide Oxidized hydrocarbons – alcohols, aldehydes, ketones and acids- is one class of common organic compounds. Pure hydrocarbons are typically hydrophobic. However, their hydrophobic nature can be changed via introducing the functional atoms/groups, such as oxygen and nitrogen. For instance, the methane and ethane are hydrophobic while formic acid and ethanol become hydrophilic when oxygen atom is introduced. The hydrophilic groups are of importance for biological molecule leading to the solubility and acid-base reactions. Table 3 shows the densities of some typical organic oxide compounds, as well as the liquid water. For each system, we put 300 molecules in the simulation box. Compared to the experimental data, the density predicted with CHON-2017_weak force field is much better than protein-2013, especially for the alcohol compounds and water. For example, the water densities are 0.90 and 0.99 g/cm^3

with protein-2013 and CHON-2017_weak force field, respectively. It is clear the CHON-2017_weak force field reproduces the experimental data well. But we also note the densities of liquid formic acid and formaldehyde are still underestimated compared to experiment data.

Table 3. Densities of the Oxides of Hydrocarbon at 298.15K.

System	Chemical formula	protein-2013	CHON-2017_weak	expt.
Formic acid	CH_2O_2	0.80	0.87	1.22[48]
formaldehyde	CH_2O	0.60	0.68	0.82[49]
methanol	CH_3OH	1.04	0.83	0.79[49]
ethanol	C_2H_5OH	1.12	0.82	0.79[50]
water	H_2O	0.87	0.99	1.00[51]

Amino acid crystal Protein is another very important class of functionalized hydrocarbon based compounds. Given the complexity of typical proteins and enzymes, it is computationally expensive to directly calculate the protein properties at the atomistic level. However, the amino acid residues are the smallest units and assemble into proteins, it is thus appropriate to validate the quality of the CHON-2017_weak force field with amino acids. Table 4 shows the densities of some typical amino acid crystals. All of the crystal structures of unit cell were reproduced from the Cambridge Crystallographic Data Center (CCDC).[36] The supercells were adopted in the ReaxFF simulations. For example, we built $4 \times 4 \times 4$ supercells for the smaller size amino acids of glycine, D-alanine and L-aspartic acid, while $3 \times 3 \times 3$ supercells for other bigger amino acids, respectively. Compared to the experimental data, the densities predicted with protein-2013 force field

are generally underestimated for small size amino acids but overestimated for the larger amino acids. The CHON-2017_weak force field shows much better prediction and the simulated densities are in agreement with the experimental results.

Table 4. Densities of the Amino Acid Crystals at 100K.

System	Chemical formula	protein-2013	CHON-2017_weak	expt.[36]
glycine	$C_2H_5NO_2$	1.54	1.64	1.61
L-aspartic acid	$C_4H_7NO_4$	1.54	1.68	1.64
L-isoleucine	$C_6H_{13}NO_2$	1.36	1.28	1.22
L-phenylalanine	$C_9H_{11}NO_2$	1.50	1.39	1.35
histidine	$C_6H_9N_3O_2$	1.68	1.67	1.52
L-arginine	$C_6H_{14}N_4O_2$	1.50	1.43	1.34
D-alanine	$C_3H_7NO_2$	1.50	1.52	1.40

From the comparison of densities predicted by protein-2013 and CHON-2017_weak force fields with experiment data for n-alkanes, aromatic hydrocarbons, hydrocarbon oxides and amino acid crystals, it is clear the CHON-2017_weak force field is much better than protein-2013 force field in the density descriptions for the pure molecule systems in the condensed phase.

3.3 Mixture models

As mentioned above, the pure hydrocarbons are hydrophobic while the oxygen or nitrogen functionalized hydrocarbon compounds are usually hydrophilic. Therefore, we set up three typical mixture models, such as hexane-water, ethanol-water and TMA-water mixtures to study their solubility in water. In these simulations, the total molecule

number is kept to 300 for each system. Since the densities of liquid hexane and ethanol are much lower than that of pure liquid water, we expect the density of mixtures should also be lower than the water. Actually, from the results in Table 5, it is indeed found the density predicted by CHON-2017_weak force field is smaller than bulk water and the value increases with the decreasing functionalized hydrocarbon mole ratio. However, the protein-2013 force field overestimates the density too much, particularly for the system in the condition of low water mole ratio. From the results of mole ratio dependence of ethanol-water mixtures, it demonstrates the trend of simulated density is consistent with experimental observation.

Table 5. Densities of the Mixture Model systems at 298.15K.

System	mole ratio	protein-2013	CHON-2017_weak	expt.[52]
hexane-water	4:1	1.02	0.68	~
	1:1	1.03	0.72	~
	1:4	1.08	0.83	~
ethanol-water	4:1	1.13	0.85	0.81
	1:1	1.12	0.93	0.85
	1:4	1.03	0.99	0.94
TMA-water	1:5	1.18	1.00	~

In order to study the phase information of the system, we illustrated the snapshots of the configurations of mixtures after 500 ps MD simulations in Figure 3. From configurations of the hexane-water mixture (Figure 3a and Figure 3b), the phase separations are observed clearly even though the water and hexane molecules were initially placed in the

simulation box randomly. That is because the hexane is hydrophobic and insoluble in water phase. However, the ethanol and TMA molecules are well soluble in water; as a result, no phase separation appears (Figure 3c, Figure 3d and Figure 3e for ethanol-water with different mole ratios, and Figure 3f for TMA-water). Our simulation results are consistent with experimental observations.[50, 53]

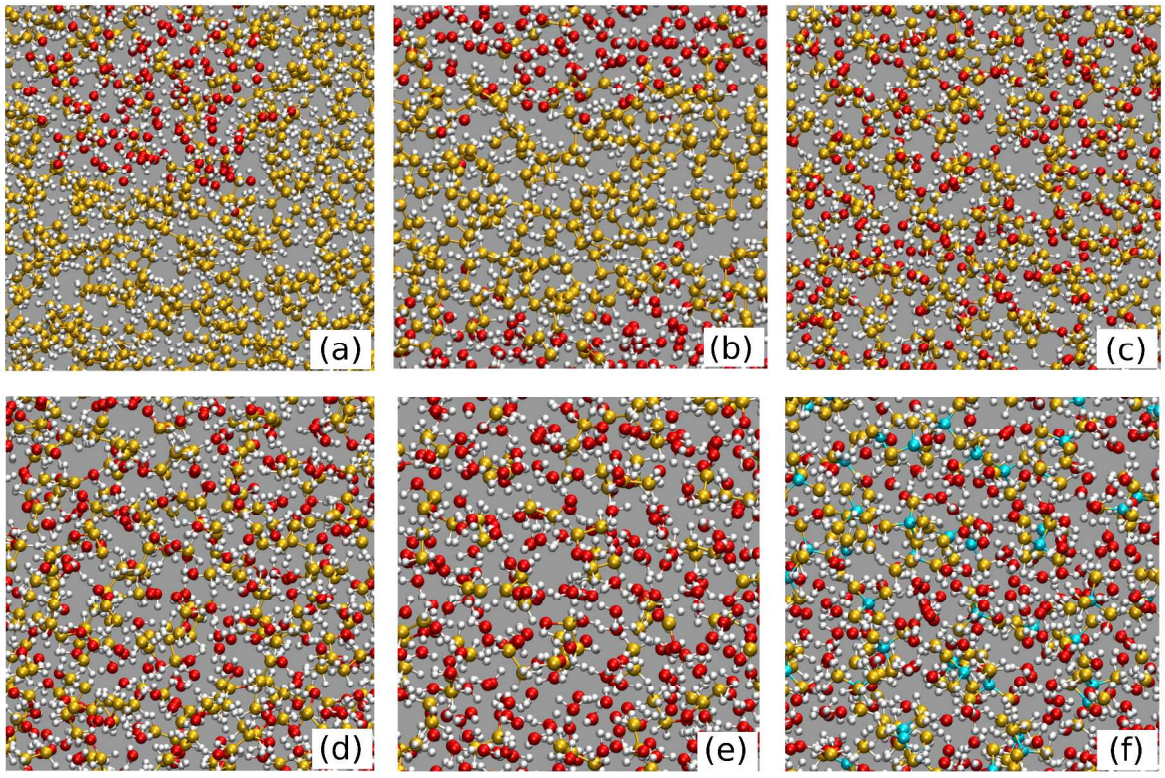

Figure 3: (a) and (b) display the configurations of hexane-water mixture with 1:1 and 1:4 mole ratios, respectively. (c), (d) and (e) show the configurations of ethanol-water mixture with 4:1, 1:1 and 1:4 mole ratios, respectively. (f) The configuration of TMA-water mixture. Oxygen is shown in red, carbon in dark orange, hydrogen in white, and nitrogen in sky blue.

It is known TMA-OH molecule is highly soluble in water[53] and quaternary ammonium is usually an important side chain for polymers in AEM fuel cell. Therefore, analyzing the structural property (i.e. RDF and coordination number) of TMA/OH/water mixture

should be helpful in understanding the property of real AEMs. To accomplish this analysis, we randomly replaced 20 water molecules with OH ions in the configurations of TMA-water mixtures and equilibrated the systems with NVT/MD simulations. Here, the hydration level of TMA/OH/water system is about 11 (λ=11, the ratio of water molecule and OH^-), which corresponds to the intermediate water uptake in the fuel cell. Figure 4 shows the comparison of RDFs simulated with protein-2013 and CHON-2017_weak force fields. From Figure 4a, we found a large right shift for the RDF of nitrogen-nitrogen in CHON-2017_weak prediction, which indicates the TMA-TMA interaction becomes weaker. Such difference is reasonable because CHON-2017_weak force field reproduces the experimental density well while the protein-2013 force field overestimates the interaction of hydrocarbon compound, as a result, the latter leads to shorter molecule-molecule distance. For the first solvation shell of TMA, as illustrated in Figure 4b, the intensity of first peak of N-O predicted with CHON-2017_weak force field is weak and broad compared to that of protein-2013, it shows the interaction between TMA and water also becomes weaker. To analyze the correlation between TMA and hydroxide ion, we calculated the RDF of $N\text{-}O^*$ (hydroxide ion) and presented it in Figure 4c. It is clear the first peak with a strong intensity calculated from protein-2013 simulations significantly decreases in the CHON-2017_weak prediction, which means the compound of [TMA][OH] can highly dissociate and the hydroxide ions are well solvated by water molecules. Furthermore, the RDF of $O^*(OH^-)\text{-}O(H_2O)$ is shown in Figure 4d. It is found both protein-2013 and CHON-2017_weak force fields show strong correlation between hydroxide ion and water molecules, and they predict the same number of water molecules binding with OH^-, as shown the coordination number (CNs) in first solvation

shell. From the comparison of CNs for N-N, N-O and N-O*, it is found the CNs with CHON-2017_weak force field are smaller than that with protein-2013 due to the decreased interaction between molecules in CHON-2017_weak simulations. However, the CN of O^*-O predicted with CHON-2017_weak increases compared to that with protein-2013 force field simulations. That is because the protein-2013 force field underestimates the interaction between water molecules, as a result, the water phase becomes more loosely connected and fewer water molecules are involved in the same large distance around a hydroxide ion. .

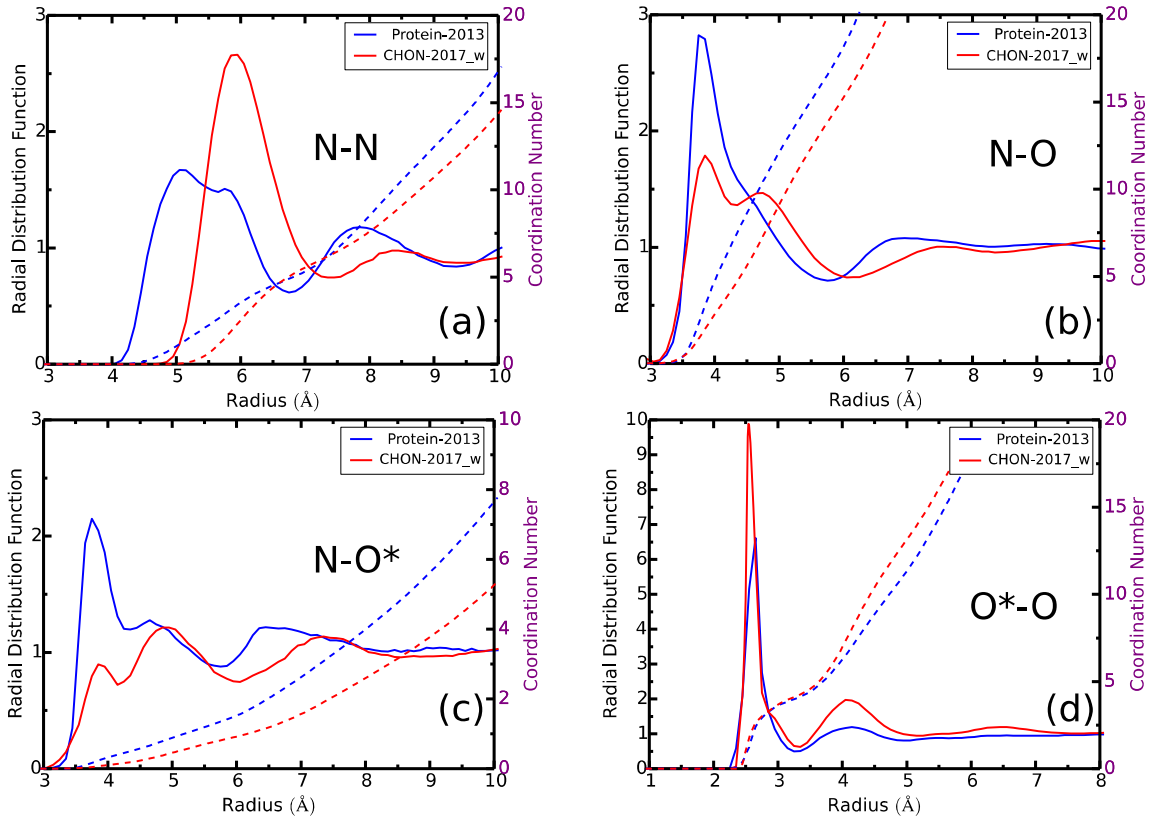

Figure 4: The radial distribution functions and coordination numbers of (a) N-N, (b) N-O, (c) N-O and (d)O*-O of TMA/OH/water mixture simulated with protein-2013 and CHON-2017_weak ReaxFF force fields.*

3.4 Reaction mechanism

Reaction between OH-anion and TMA molecule The degradation mechanism of TMA cation is of interest in the studies of anion exchange membrane (AEM) fuel cells and the protein-2013 force field was successfully used to investigate the structural and transport properties of AEM, as well as the chemical stability.[32] Therefore, here we took the reaction of OH-anion with TMA molecules for example to validate the quality of CHON-2017_weak force field. It is known that there are two main different mechanisms for degradation of membrane in fuel cells, namely S_N2 and ylide reactions, as shown in Figure 5.[54] In this work, since we are interested in the liquid phase reactions and the previous DFT calculations implemented with polarizable continuum model (PCM) were employed to study the degradation mechanism,[55-56] we therefore take the solvated OH^- with three water molecules as the model system in our ReaxFF simulations to account for the chemical environment effect. The configurations of reactants, transition states and products are depicted in Figure 5a and Figure 5b for S_N2 and ylide reactions, respectively. DFT calculations carried out at B3LYP/6-311++G(2d, p) level show that the S_N2 reaction is thermodynamically downhill (ΔG = -28.7 kcal/mol) with a reaction barrier of 17.0 kcal/mol, and the reaction barrier is only 9.2 kcal/mol for the ylide (hydrogen abstraction) thermodynamically uphill pathway.[56] Using the current CHON-2017_weak force field, the ReaxFF predicts the barriers of 13.67 and 5.18 kcal/mol for the S_N2 and ylide reactions, respectively. As shown in Figure 5d, although the reaction barrier of ReaxFF is lower than the DFT data about several kcal/mol, one expects that the reaction barrier would increase by a few kcal/mol when more additional water molecules are involved.[56-57] Furthermore, the ReaxFF can also correctly produce that the S_N2 and ylide reactions are thermodynamically favorable and unfavorable referring to the energy of

-29.48 and 4.96 kcal/mol, respectively.

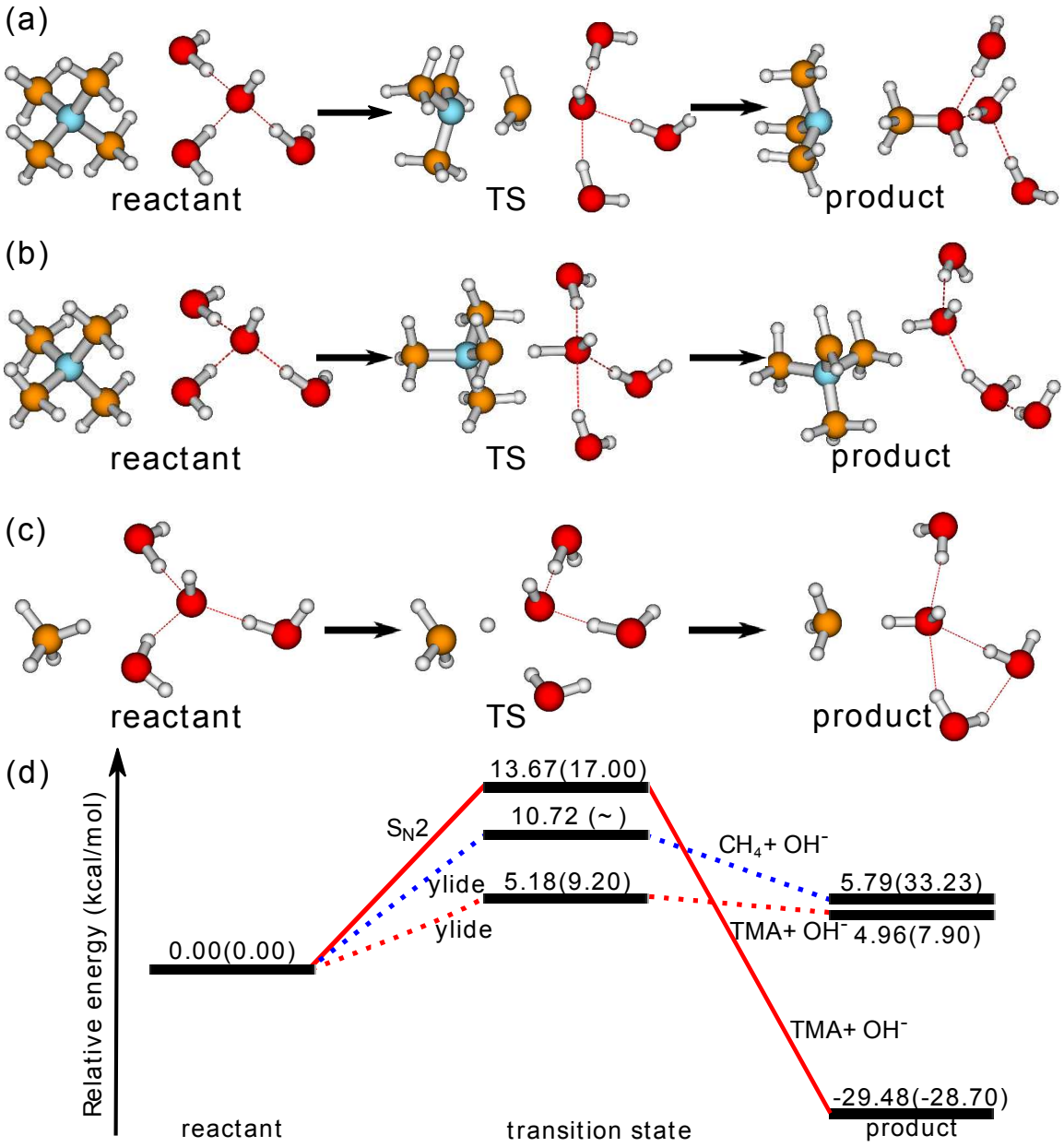

Figure 5: (a) The configurations of reactant, transition state and product for the S_N2 reaction path of OH^- and TMA. (b) The configurations of reactant, transition state and product for the ylide reaction path of OH^- and TMA. (c) The configurations of reactant, transition state and product for the hydrogen abstraction reaction path of OH^- and methane. Oxygen is shown in red, carbon in dark orange, hydrogen in white, and

nitrogen in sky blue. (d) ReaxFF energy levels of the stationary points along the reaction coordinate for the reactions of OH^- with TMA and CH_4. The data in parentheses are of DFT calculations. No transition state was found for the reaction of OH^- with CH_4.

Hydrogen abstraction for OH-anion from methane In contrast with popular non-reactive force fields such as AMBER and CHARMM etc., in which one element may has different parameters depending on its chemical environment, there is only one atom type in ReaxFF for each regardless of the chemical environment in which the atom finds itself.[1] So ReaxFF has the ability to give a unified description for a particular element. In Figure 5b, hydrogen abstraction refers to alpha-hydrogen in the reaction of OH^- with TMA, which is hydrophilic. Here, we selected methane to study to the hydrogen abstraction reaction for OH^- from hydrophobic compounds (Figure 5c). Compared to the results of reaction of OH^- with TMA, the ReaxFF simulations predict the energy barrier is much higher (10.72 kcal/mol) and the reaction becomes more unfavorable thermodynamically (5.79 kcal/mol), as shown in Figure 5d. Although the relative energy of product is much lower than the DFT result at BHandHLYP/6-311++G(2d,p) level with PCM model (33.23 kcal/mol, endothermic reaction without energy barrier), which functional performs well for the study of hydrogen abstraction reaction for OH radical,[58] such reaction is also unfavorable in ReaxFF due to the fact that the high reaction barrier, and the OH^- is hydrophilic and as such likely to be solvated in the water phase. We should mention that our ReaxFF predicts the reaction of unsolvated OH^- with methane (i.e. gas phase reaction) to be an exothermic reaction, which releases the energy of 6.37 kcal/mol with a barrier of 7.56 kcal/mol, where the OH-anion performs like the OH radical, which releases the energy of 8.99 kcal/mol with a barrier of 10.50 kcal/mol at

BHandHLYP/6-311++G(2d,p) level.

Degradation of TMA in alkaline aqueous solution In AEM fuel cells, the degradation is usually investigated at a relative high temperature, for example 60℃ in experiment.[59] Therefore, we ran the ReaxFF MD simulation at 400K rather than at room temperature to study the degradation of the TMA. There are 50 TMA molecules, 50 OH^- and 200 water molecules in the system, where a very low hydration level (λ=4) was examined to accelerate the reactions. The main degradation pathway is shown in Figure 6. Firstly, an OH^- molecule approaches the TMA during MD simulation, and then it abstracts one hydrogen atom from TMA at a proper position. As a result, the generated water molecule moves away and allow the second OH^- to attack the under-coordinated -CH_2 group. Once the second OH^- attaches to the TMA molecule, it is likely to release its hydrogen to the third OH^- molecule. Eventually, the bond breaking is observed between nitrogen and carbon because of the over-coordination of carbon. Although the DFT calculation supports the S_N2 degradation pathway due to the same product observation as experiment,[55] we found the ylide reaction pathway is more favorable in aqueous solution, because the energy barrier of hydrogen shift reaction is much lower than that of S_N2 reaction. Furthermore, the multi-OH anion attack pathway can also induce the experimentally observed degradation arising from the carbon-nitrogen bond breaking.

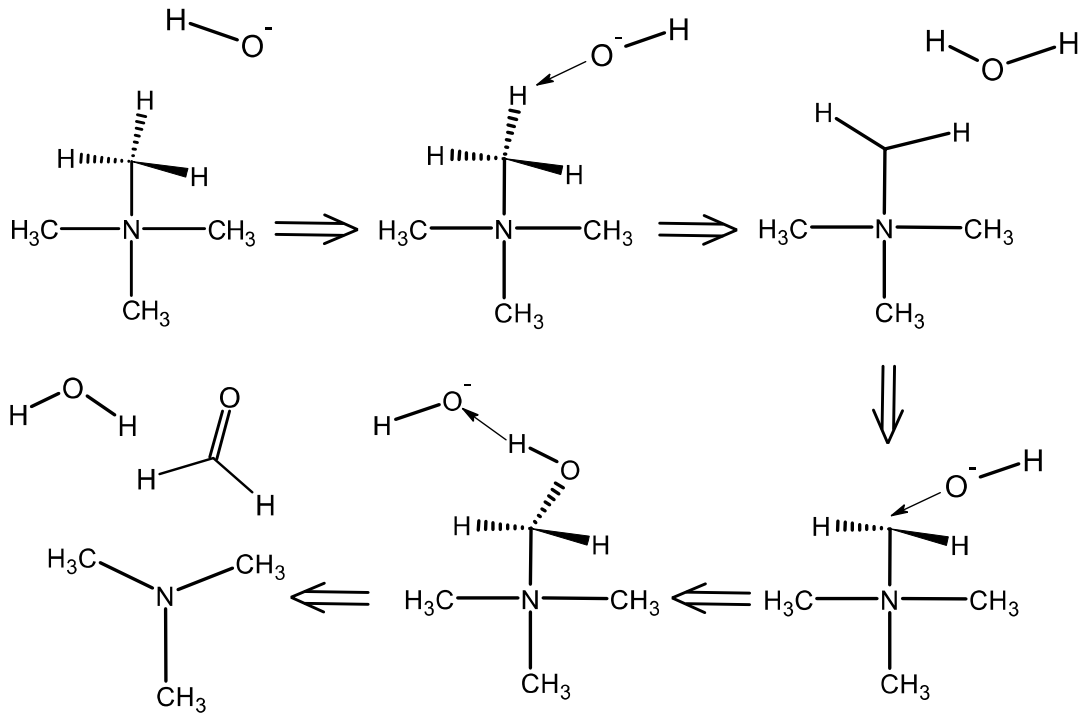

Figure 6: The main degradation pathway of TMA in basic aqueous solution. The multi-OH anion attack induces CH_2O formation.

4 Conclusions

In this paper, we presented the development of a new generation ReaxFF force field (CHON-2017_weak) to describe the functionalized hydrocarbon/water weak interactions in the condensed phase. The parameters of force field are retrained on the basis of our previous protein force field (protein-2013). From the analyses of the results and comparisons with experimental data, it indicates that the CHON-2017_weak force field is essentially improved for the predictions of the densities of a series of modeling systems, such as n-alkane compounds, aromatic hydrocarbons, oxides of hydrocarbon, amino acid crystals, as well as some mixture modeling systems such as hexane-water, ethanol-water and TMA-water. For the mixture systems, we observed the phase separation phenomenon in hexane-water system due to the hydrophobic characteristic of hexane, but no phase

separation in ethanol-water and TMA-water mixtures as expected, because hydrophobic hydrocarbons become hydrophobic and highly soluble in water when they are functionalized by oxygen or nitrogen. Moreover, the CHON-2017_weak force field predicts the similar reaction barrier with quantum mechanics calculations for the model systems.

From our ReaxFF MD simulation of the degradation of TMA in aqueous solution, we found the ylide reaction is much more favorable energetically than S_N2 reaction taking place in solution due to the lower energy barrier of the hydrogen abstraction reaction. The multi-OH anion attack finally induces the carbon-nitrogen bond breaking in TMA molecule. Such additional degradation pathway with low reaction barrier is more favorable than S_N2 reaction, which barrier is up to ~20 kcal/mol. In hydrated AEMs functionalized with quaternary ammonium cation groups, the hydroxide transport in the hydrophilic phase and the chemical degradation of membrane are the major considerations in the design of high-performance AEM fuel cells in experiment. Both of them strongly depend on the cation groups similar to TMA. The present results thus are helpful for us to understand the properties of realistic AEMs such as structural and dynamic properties, as well as their chemical stability.

AUTHOR INFORMATION

Corresponding Authors

*E-mail: acv13@psu.edu. Tel: +1-814-863-6277.

Notes

The authors declare no competing financial interest.

Acknowledgments

This work was supported by a grant from the U.S. Army Research Laboratory through the Collaborative Research Alliance (CRA) for Multi Scale Multidisciplinary Modeling of Electronic Materials (MSME).

Supporting Information

The ReaxFF reactive force field parameters of CHON-2017_weak were used in the present work. This information is available free of charge via the Internet at http://pubs.acs.org

References

1. Senftle, T. P.; Hong, S.; Islam, M. M.; Kylasa, S. B.; Zheng, Y.; Shin, Y. K.; Junkermeier, C.; Engel-Herbert, R.; Janik, M. J.; Aktulga, H. M.; et al., The ReaxFF Reactive Force-Field: Development, Applications and Future Directions. *npj Comput. Mater.* **2016**, *2*, 15011.
2. Monticelli, L.; Tieleman, D. P., Force Fields for Classical Molecular Dynamics. *Methods Mol. Biol.* **2013**, 197-213.
3. González, M., Force Fields and Molecular Dynamics Simulations. *Collection SFN* **2011**, *12*, 169-200.
4. Mark, J. E., *Physical Properties of Polymers Handbook*; Springer, 2007; Vol. 1076.
5. Allinger, N. L., Conformational Analysis. 130. MM2. A Hydrocarbon Force Field Utilizing V1 and V2 Torsional Terms. *J. Am. Chem. Soc.* **1977**, *99*, 8127-8134.
6. Allinger, N. L.; Yuh, Y. H.; Lii, J. H., Molecular Mechanics. The MM3 Force Field for Hydrocarbons. 1. *J. Am. Chem. Soc.* **1989**, *111*, 8551-8566.
7. Rappé, A. K.; Casewit, C. J.; Colwell, K.; Goddard III, W.; Skiff, W., UFF, a Full Periodic Table Force Field for Molecular Mechanics and Molecular Dynamics Simulations. *J. Am. Chem. Soc.* **1992**, *114*, 10024-10035.
8. Mayo, S. L.; Olafson, B. D.; Goddard, W. A., Dreiding: A Generic Force Field for Molecular Simulations. *J. Phys. Chem.* **1990**, *94*, 8897-8909.
9. Oostenbrink, C.; Villa, A.; Mark, A. E.; Van Gunsteren, W. F., A Biomolecular Force Field Based on the Free Enthalpy of Hydration and Solvation: The Gromos Force-Field Parameter Sets 53A5 and 53A6. *J. Comput. Chem.* **2004**, *25*, 1656-1676.
10. Cornell, W. D.; Cieplak, P.; Bayly, C. I.; Gould, I. R.; Merz, K. M.; Ferguson, D. M.; Spellmeyer, D. C.; Fox, T.; Caldwell, J. W.; Kollman, P. A., A Second Generation Force Field for the Simulation of Proteins, Nucleic Acids, and Organic Molecules. *J. Am. Chem. Soc.* **1995**, *117*, 5179-5197.
11. MacKerell Jr, A. D.; Bashford, D.; Bellott, M.; Dunbrack Jr, R. L.; Evanseck, J. D.; Field, M. J.; Fischer, S.; Gao, J.; Guo, H.; Ha, S.; et al., All-Atom Empirical Potential for Molecular Modeling and Dynamics Studies of Proteins. *J. Phys. Chem. B* **1998**, *102*, 3586-3616.
12. Jorgensen, W. L.; Maxwell, D. S.; Tirado-Rives, J., Development and Testing of the OPLS All-Atom Force Field on Conformational Energetics and Properties of Organic Liquids. *J. Am. Chem. Soc.* **1996**, *118*, 11225-11236.
13. Sun, H., Compass: An ab Initio Force-Field Optimized for Condensed-Phase Applications Overview with Details on Alkane and Benzene Compounds. *J. Phys. Chem. B* **1998**, *102*, 7338-7364.
14. Jorgensen, W. L.; Chandrasekhar, J.; Madura, J. D.; Impey, R. W.; Klein, M. L., Comparison of Simple Potential Functions for Simulating Liquid Water. *J. Chem. Phys.* **1983**, *79*, 926-935.

15. Jorgensen, W. L.; Jenson, C., Temperature Dependence of TIP3P, SPC, and TIP4P Water from NPT Monte Carlo Simulations: Seeking Temperatures of Maximum Density. *J. Comput. Chem.* **1998**, *19*, 1179-1186.
16. Abascal, J. L.; Vega, C., A General Purpose Model for the Condensed Phases of Water: TIP4P/2005. *J. Chem. Phys.* **2005**, *123*, 234505.
17. Liang, T.; Shin, Y. K.; Cheng, Y.-T.; Yilmaz, D. E.; Vishnu, K. G.; Verners, O.; Zou, C.; Phillpot, S. R.; Sinnott, S. B.; van Duin, A. C., Reactive Potentials for Advanced Atomistic Simulations. *Annu. Rev. Mater. Res.* **2013**, *43*, 109-129.
18. Brenner, D. W., Empirical Potential for Hydrocarbons for Use in Simulating the Chemical Vapor Deposition of Diamond Films. *Phys. Rev. B* **1990**, *42*, 9458.
19. Yu, J.; Sinnott, S. B.; Phillpot, S. R., Charge Optimized Many-Body Potential for the Si/SiO2 System. *Phys. Rev. B* **2007**, *75*, 085311.
20. van Duin, A. C.; Dasgupta, S.; Lorant, F.; Goddard, W. A., ReaxFF: A Reactive Force Field for Hydrocarbons. *J. Phys. Chem. A* **2001**, *105*, 9396-9409.
21. Ashraf, C.; van Duin, A. C., Extension of the ReaxFF Combustion Force Field toward Syngas Combustion and Initial Oxidation Kinetics. *J. Phys. Chem. A* **2017**, *121*, 1051-1068.
22. van Duin, A. C.; Strachan, A.; Stewman, S.; Zhang, Q.; Xu, X.; Goddard, W. A., ReaxFFsio Reactive Force Field for Silicon and Silicon Oxide Systems. *J. Phys. Chem. A* **2003**, *107*, 3803-3811.
23. Wen, J.; Ma, T.; Zhang, W.; van Duin, A. C.; Lu, X., Surface Orientation and Temperature Effects on the Interaction of Silicon with Water: Molecular Dynamics Simulations Using ReaxFF Reactive Force Field. *J. Phys. Chem. A* **2017**, *121*, 587-594.
24. Fogarty, J. C.; Aktulga, H. M.; Grama, A. Y.; Van Duin, A. C.; Pandit, S. A., A Reactive Molecular Dynamics Simulation of the Silica-Water Interface. *J. Chem. Phys.* **2010**, *132*, 174704.
25. van Duin, A. C.; Bryantsev, V. S.; Diallo, M. S.; Goddard, W. A.; Rahaman, O.; Doren, D. J.; Raymand, D.; Hermansson, K., Development and Validation of a ReaxFF Reactive Force Field for Cu Cation/Water Interactions and Copper Metal/Metal Oxide/Metal Hydroxide Condensed Phases. *J. Phys. Chem. A* **2010**, *114*, 9507-9514.
26. Raymand, D.; van Duin, A. C.; Spångberg, D.; Goddard, W. A.; Hermansson, K., Water Adsorption on Stepped ZnO Surfaces from MD Simulation. *Surf. Sci.* **2010**, *604*, 741-752.
27. Pitman, M. C.; van Duin, A. C., Dynamics of Confined Reactive Water in Smectite Clay–Zeolite Composites. *J. Am. Chem. Soc.* **2012**, *134*, 3042-3053.
28. Monti, S.; Corozzi, A.; Fristrup, P.; Joshi, K. L.; Shin, Y. K.; Oelschlaeger, P.; van Duin, A. C.; Barone, V., Exploring the Conformational and Reactive Dynamics of Biomolecules in Solution Using an Extended Version of the Glycine Reactive Force Field. *Phys. Chem. Chem. Phys.* **2013**, *15*, 15062-15077.
29. Chenoweth, K.; van Duin, A. C.; Goddard, W. A., ReaxFF Reactive Force Field for Molecular Dynamics Simulations of Hydrocarbon Oxidation. *J. Phys. Chem. A* **2008**, *112*, 1040-1053.
30. van Duin, A. C. T.; Zou, C.; Joshi, K.; Bryantsev, V.; Goddard, W. A., Chapter 6 a ReaxFF Reactive Force-Field for Proton Transfer Reactions in Bulk Water and Its Applications to Heterogeneous Catalysis. In *Computational Catalysis*, The Royal Society of Chemistry: 2014; pp 223-243.
31. Rahaman, O.; van Duin, A. C.; Goddard III, W. A.; Doren, D. J., Development of a ReaxFF Reactive Force Field for Glycine and Application to Solvent Effect and Tautomerization. *J. Phys. Chem. B* **2010**, *115*, 249-261.
32. Zhang, W.; van Duin, A. C., ReaxFF Reactive Molecular Dynamics Simulation of Functionalized Poly (Phenylene Oxide) Anion Exchange Membrane. *J. Phys. Chem. C* **2015**, *119*, 27727-27736.
33. van Duin, A. C.; Baas, J. M.; van de Graaf, B., Delft Molecular Mechanics: A New Approach to Hydrocarbon Force Fields. Inclusion of a Geometry-Dependent Charge Calculation. *J. Chem. Soc., Faraday Trans.* **1994**, *90*, 2881-2895.
34. Te Velde, G. t.; Bickelhaupt, F. M.; Baerends, E. J.; Fonseca Guerra, C.; van Gisbergen, S. J.; Snijders, J. G.; Ziegler, T., Chemistry with ADF. *J. Comput. Chem.* **2001**, *22*, 931-967.
35. Plimpton, S., Fast Parallel Algorithms for Short-Range Molecular Dynamics. *J. Comput. Phys.* **1995**, *117*, 1-19.
36. Groom, C. R.; Bruno, I. J.; Lightfoot, M. P.; Ward, S. C., The Cambridge Structural Database. *Acta Crystallogr. Sect. B: Struct. Sci.* **2016**, *72*, 171-179.

37. Zhang, W.; van Duin, A. C., Second-Generation ReaxFF Water Force Field: Improvements in the Description of Water Density and OH-Anion Diffusion. *J. Phys. Chem. B* **2017**, 121, 6021-6032.
38. Soper, A., The Radial Distribution Functions of Water and Ice from 220 to 673 K and at Pressures up to 400 MPa. *Chem. Phys.* **2000**, *258*, 121-137.
39. Huang, C.; Wikfeldt, K.; Nordlund, D.; Bergmann, U.; McQueen, T.; Sellberg, J.; Pettersson, L. G.; Nilsson, A., Wide-Angle X-Ray Diffraction and Molecular Dynamics Study of Medium-Range Order in Ambient and Hot Water. *Phys. Chem. Chem. Phys.* **2011**, *13*, 19997-20007.
40. Afonine, P.; Urzhumtsev, A., On a Fast Calculation of Structure Factors at a Subatomic Resolution. *Acta Crystallogr. Sect. A: Found. Crystallogr.* **2004**, *60*, 19-32.
41. Mancinelli, R.; Botti, A.; Bruni, F.; Ricci, M.; Soper, A., Perturbation of Water Structure Due to Monovalent Ions in Solution. *Phys. Chem. Chem. Phys.* **2007**, *9*, 2959-2967.
42. Audonnet, F.; Pádua, A. A., Simultaneous Measurement of Density and Viscosity of N-Pentane from 298 to 383 K and up to 100 MPa Using a Vibrating-Wire Instrument. *Fluid Phase Equilib.* **2001**, *181*, 147-161.
43. Aminabhavi, T.; Patil, V.; Aralaguppi, M.; Phayde, H., Density, Viscosity, and Refractive Index of the Binary Mixtures of Cyclohexane with Hexane, Heptane, Octane, Nonane, and Decane at (298.15, 303.15, and 308.15) K. *J. Chem. Eng. Data* **1996**, *41*, 521-525.
44. Kashiwagi, H.; Hashimoto, T.; Tanaka, Y.; Kubota, H.; Makita, T., Thermal Conductivity and Density of Toluene in the Temperature Range 273–373 K at Pressures up to 250 MPa. *Inter. J. Thermophys.* **1982**, *3*, 201-215.
45. Schobert, H., *Chemistry of Fossil Fuels and Biofuels*; Cambridge University Press, 2013.
46. Patnode, W.; Scheiber, W., The Density, Thermal Expansion, Vapor Pressure, and Refractive Index of Styrene, and the Density and Thermal Expansion of Polystyrene. *J. Am. Chem. Soc.* **1939**, *61*, 3449-3451.
47. Asfour, A. F. A.; Siddique, M. H.; Vavanellos, T. D., Density-Composition Data for Eight Binary Systems Containing Toluene or Ethylbenzene and C8-C16 N-Alkanes at 293.15, 298.15, 308.15, and 313.15 K. *J. Chem. Eng. Data* **1990**, *35*, 192-198.
48. Brar, S. K.; Sarma, S. J.; Pakshirajan, K., *Platform Chemical Biorefinery: Future Green Chemistry*; Elsevier, 2016.
49. Darling, D.; Schulze-Makuch, D., *The Extraterrestrial Encyclopedia*; First Edition Design Pub., 2016.
50. Haynes, W. M., Bruno, T. J., Lide, D. R., Eds. *CRC Handbook of Chemistry and Physics*; 96th ed., CRC press: Boca Raton, FL, 2016.
51. Riddick, J. A.; Bunger, W. B.; Sakano, T. K., Organic Solvents, 3rd ed., Wiley-Interscience: New York, **1986**.
52. Solutions For Technicians: Density and Concentraton Calculator for Mixtures of Ethanool and Water at 20 ^{o}C. www.handymath.com/cgi-bin/ethanolwater3.cgi?submit=Entry (accessed March 7, 2018).
53. Lin, C.-C.; Yang, C.-C.; Ger, J.; Deng, J.-F.; Hung, D.-Z., Tetramethylammonium Hydroxide Poisoning. *Clin. toxicol.* **2010**, *48*, 213-217.
54. Macomber, C.; Boncella, J.; Pivovar, B.; Rau, J., Decomposition Pathways of an Alkaline Fuel Cell Membrane Material Component Via Evolved Gas Analysis. *J. Therm. Anal. Calorim.* **2008**, *93*, 225-229.
55. Chempath, S.; Einsla, B. R.; Pratt, L. R.; Macomber, C. S.; Boncella, J. M.; Rau, J. A.; Pivovar, B. S., Mechanism of Tetraalkylammonium Headgroup Degradation in Alkaline Fuel Cell Membranes. *J. Phys. Chem. C* **2008**, *112*, 3179-3182.
56. Chempath, S.; Boncella, J. M.; Pratt, L. R.; Henson, N.; Pivovar, B. S., Density Functional Theory Study of Degradation of Tetraalkylammonium Hydroxides. *J. Phys. Chem. C* **2010**, *114*, 11977-11983.
57. Dekel, D. R.; Amar, M.; Willdorf, S.; Kosa, M.; Dhara, S.; Diesendruck, C. E., Effect of Water on the Stability of Quaternary Ammonium Groups for Anion Exchange Membrane Fuel Cell Applications. *Chem. Mater.* **2017**, *29*, 4425-4431.
58. Galano, A.; Alvarez-Idaboy, J. R.; Bravo-Pérez, G.; Ruiz-Santoyo, M. E., Gas Phase Reactions of C1–C4 Alcohols with the OH Radical: A Quantum Mechanical Approach. *Phys. Chem. Chem. Phys.* **2002**, *4*, 4648-4662.
59. Arges, C. G.; Ramani, V., Investigation of Cation Degradation in Anion Exchange Membranes Using Multi-Dimensional Nmr Spectroscopy. *J. Electrochem. Soc.* **2013**, *160*, F1006-F1021.

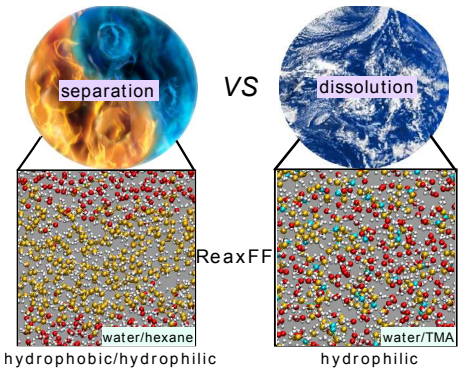
separation
VS
dissolution
ReaxFF
water/hexane
water/TMA
hydrophobic/hydrophilic
hydrophilic

TOC Graphic